NIH Public Access
Author Manuscript
J Phys Chem B. Author manuscript; available in PMC 2011 November 4.

Published in final edited form as:
J Phys Chem B. 2010 November 4; 114(43): 13872–13880. doi:10.1021/jp105718r.

On the performance of Spin Diffusion NMR Techniques in Oriented Solids: Prospects for Resonance Assignments and Distance Measurements from Separated Local Field Experiments

Nathaniel J. Traaseth[2], **T. Gopinath**[2], and **Gianluigi Veglia**[1,2,*]

[1]Department of Chemistry University of Minnesota, Minneapolis, Minnesota 55455

[2]Department of Biochemistry, Molecular Biology, and Biophysics, University of Minnesota, Minneapolis, Minnesota 55455

Abstract

NMR spin diffusion experiments have the potential to provide both resonance assignment and internuclear distances for protein structure determination in oriented solid-state NMR. In this paper, we compared the efficiencies of three common spin diffusion experiments: proton-driven spin diffusion (PDSD), cross-relaxation driven spin diffusion (CRDSD), and proton-mediated proton transfer (PMPT). As model systems for oriented proteins, we used single crystals of *N*-acetyl-L-^{15}N-leucine (NAL) and *N*-acetyl-L-^{15}N-valyl-L-^{15}N-leucine (NAVL) to probe long- and short distances, respectively. We demonstrate that for short ^{15}N/^{15}N distances such as those found in NAVL (3.3 Å), the PDSD mechanism gives the most intense cross-peaks, while for longer distances (> 6.5 Å), the CRDSD and PMPT experiments are more efficient. The PDSD was highly inefficient for transferring magnetization across distances greater than 6.5 Å (NAL crystal sample), due to small ^{15}N/^{15}N dipolar couplings (< 4.5 Hz). Interestingly, the mismatched Hartmann-Hahn condition present in the PMPT experiment gave more intense cross-peaks for lower ^{1}H and ^{15}N spinlock field strengths (32 and 17 kHz, respectively) rather than higher values (55 and 50 kHz), suggesting a more complex magnetization transfer mechanism. Numerical simulations are in good agreement with the experimental findings, suggesting a combined PMPT and CRDSD effect. We conclude that in order to assign SLF spectra and measure short and long-range distances, the combined use of homonuclear correlation spectra, such as the ones surveyed in this work, are necessary.

Keywords

NMR; solid-state NMR; NMR crystallography; spin diffusion; crystals; proton driven spin diffusion; cross-relaxation driven spin diffusion; proton-mediated proton transfer; PISEMA; HIMSELF; SAMPI4; assignment methods; *N*-acetyl-leucine; *N*-acetyl-valyl-leucine

*Author for correspondence: Gianluigi Veglia 6-155 Jackson Hall 321 Church St SE Minneapolis, MN 55455 Phone: (612) 625 0758 vegli001@umn.edu.

Supporting Information A table showing all the homonuclear and heteronuclear dipolar couplings used in the simulations (Figure 13) and supporting information for Figures 4 and 5 that plot the PDSD cross-peak intensity divided by the diagonal peak intensity for NAL and NAVL, respectively. Also, supporting information for Figures 10 and 12 are provided that plot all cross-peak intensities for both the value of the ^{1}H spinlock and the percentage of MMHH for the PMPT experiment.

NIH-PA Author Manuscript
NIH-PA Author Manuscript
NIH-PA Author Manuscript

NIH-PA Author Manuscript

NIH-PA Author Manuscript

NIH-PA Author Manuscript

Introduction

Oriented solid-state NMR is an important technique that allows anisotropic NMR parameters such as chemical shift (CS) and dipolar coupling (DC) to be measured directly.[1] This methodology has been important in resolving the orientation and structure of liquid crystalline molecules as well as in the determination of the structure and topology of membrane proteins within lipid bilayers.[1–11] To accurately probe membrane protein topology, separated local field (SLF) experiments such as PISEMA,[12, 13] SAMPI4,[14] HIMSELF,[15] and their sensitivity-enhanced variants[16–18] are used to measure DC and CS. These observables are then incorporated into structural refinement protocols essentially as dihedral angle restraints.[7, 19–21]

For membrane proteins, SLF-type spectra are assigned using selectively and/or uniformly labeled samples that rely on the periodic nature of the DC and CS (polar index slant angle, PISA, wheel pattern,[22, 23]) that results from the periodicity of secondary structures (helices and sheets) commonly present in membrane proteins.[24, 25] While this has been useful in assigning resonances for structural restraints, this approach heavily relies on the assumption of helix ideality (e.g., ideal dihedral angles for α-helices) as well as the use of several selectively labeled samples. Although membrane helix ideality has been shown to constitute a good approximation,[26] deviations can lead to incorrect assignments and a general bias toward ideal structures. Therefore, sequential assignment strategies such as those employed in solution NMR or magic angle spinning (MAS) techniques are preferred.[27–29] Unfortunately, membrane protein dynamics and mosaic spread[30] in mechanically aligned lipid bilayer samples result in severe inhomogenous line-broadening (10–15 ppm in ^{15}N linewidths).[31, 32] The implementation of magnetically aligned lipid bicelles have overcome many of the limitations in glass plate samples such as a maintaining a constant level of hydration,[2, 5, 33, 34] which has substantially decreased mosaic spread and led to increases in signal to noise and sample reproducibility.

There are three NMR experiments currently used to correlate internuclear distances in oriented solid-state NMR: proton driven spin diffusion (PDSD),[35, 36] cross-relaxation driven spin diffusion (CRDSD),[37] and proton-mediated proton transfer (PMPT)[38] (Figure 1). The preparation periods (90° and cross-polarization) and t_1 chemical shift evolution of these pulse sequences are identical (Figure 1), with the only difference occurring in the mixing elements used for spin diffusion. The PDSD contains a mixing element with no RF fields applied to either nuclei. This experiment has had limited application to membrane proteins mechanically aligned on glass plates,[39, 40] and are widely believed to be too inefficient for resonance assignment. For these reasons, two exchange sequences, CRDSD[37] and PMPT[38] (similar to PAR experiments in MAS[41–43]) were developed. The mixing period for the CRDSD experiment utilizes a weak spinlock field on ^{15}N to *drive* the spin diffusion among the ^{15}N nuclei, while the PMPT sequence, in addition to the Z-filter, contains a cross-polarization element mismatched with respect to the perfect Hartmann-Hahn condition. The PMPT experiment was recently shown to be useful in assigning SLF spectra for Pf1 phage coat protein.[44]

In oriented solid-state NMR, there has not been a parallel comparison of the three spin diffusion methods on the same system. The CRDSD experiment was tested with a single crystal of the dipeptide N-acetyl-L-^{15}N-valyl-L-^{15}N-leucine (NAVL), while PMPT was originally evaluated using a crystal of N-acetyl-L-^{15}N-leucine (NAL). These crystals differ in the nearest interatomic distances between ^{15}N spins: 3.3 and 6.5 Å for NAVL and NAL, respectively. In this study we systematically assessed the efficiency of PDSD, CRDSD and PMPT with both NAL and NAVL crystals. We found that the PDSD is the most efficient for

NIH-PA Author Manuscript

NIH-PA Author Manuscript

NIH-PA Author Manuscript

short distances and for assignment, while CRDSD and PMPT are more suitable for longer distance correlations.

Experimental Methods

NMR Spectroscopy

^{15}N labeled single crystals of NAL and NAVL were prepared by slow evaporation from H_2O as previously described.45 NMR experiments were conducted on a VNMRS Varian system operating at a ^{1}H Larmor frequency of 700 MHz. The two crystals were placed in arbitrary orientations with respect to the magnetic field in order to maximize the dispersion of ^{15}N resonances. All spin diffusion experiments were conducted on the same crystal orientations using a double resonance low-E probe.46 For all experiments, including the PISEMA, PDSD, CRDSD, and PMPT (see Figure 1), 4 or 16 scans (NAL or NAVL, respectively) were acquired for each t_1 increment with a 3 sec recycle delay between experiments. The spectral widths for the homonuclear ^{15}N/^{15}N spectra were 10 and 50 kHz for the indirect and direct dimensions with a total acquisition time of 4 and 10 ms, respectively. For the PDSD experiments, we employed mixing periods from 1 to 30 sec for NAL and 1 to 20 sec for NAVL. The ^{15}N radiofrequency driven spin diffusion (RFDSD)47, 48 experiments were conducted by varying the ^{15}N spinlock field ($\omega_s/2\pi$) from 0 to 50 kHz with no proton spinlock. The CRDSD experiments37 were then performed by adjusting the mixing time from 1 to 20 msec using a ^{15}N spinlock of 21 kHz (optimized value). For the PMPT experiments,38 three variables were adjusted. First, spectra were acquired by varying the ^{1}H spinlock field ($\omega_I/2\pi$) during mismatch-Hartmann-Hahn (mmHH) from 0 to 70 kHz at three ^{15}N spinlock fields ($\omega_S/2\pi$ = 21, 37.5, and 52.5 kHz) at a mixing time of 10 msec. The ^{1}H spinlock fields that gave the most intense cross-peaks were used when performing mixing time build-up curves from 1 to 20 msec. All 2D experiments were acquired in a pseudo-3D interleaved fashion to minimize experimental errors.

Numerical Simulations

PMPT and CRDSD experiments were simulated by considering 12 spins (two ^{15}N, spin *S* and 10 ^{1}H nuclei, spin *I*). The rotating frame Hamiltonian in the presence of on-resonance RF pulses on *I* and *S* spins is given by:

$$\begin{aligned} H= &\ \omega_s (S_{1x}+S_{2x}) + \omega_1 \sum_{i=1}^{N} I_{ix} + H_{IS} + H_{II} + H_{SS} \\ H_{IS} &= \sum_{i=1}^{N} [d_{1i} S_{1z} I_{iz} + d_{2i} S_{2z} I_{iz}] \\ H_{II} &= \sum_{i<j}^{N} b_{1i} \left[I_{iz} I_{jz} - \tfrac{1}{4} \left(I_{+i} I_{-j} + I_{-i} I_{+j} \right) \right] \\ H_{SS} &= b_{12} \left[S_{iz} S_{2z} - \tfrac{1}{4} (S_{+1} S_{-2} + S_{-1} S_{+2}) \right] \end{aligned} \quad (1)$$

H_{IS} is the heteronuclear dipolar Hamiltonian, H_{II} and H_{SS} are the homonuclear dipolar Hamiltonians, ω_I and ω_S are RF amplitudes for spins *I* and *S*, and d_{ij} and b_{ij} are the hetero and homonuclear dipolar couplings between nuclei *i* and *j*, respectively. The simulations were carried out with $N = 10$. In order to calculate all d_{ij} and b_{ij} values for NAL, we performed a PISEMA experiment to measure CS and DC values for the four unique ^{15}N sites. These observables were then used to rotate the crystal coordinate file of NAL (CCDC 624793) to best match the experimental values. After optimization, two ^{15}N nuclei were chosen that had the closest distances in the crystal (6.5 Å), corresponding to a ^{15}N/^{15}N dipolar coupling of 3.2 Hz. In addition, 10 protons were selected that had > 30 Hz dipolar couplings with both ^{15}N nuclei. All dipolar couplings used for the simulation are given in the Supplementary Table II. In order to calculate the transfer efficiency between the two ^{15}N

NIH-PA Author Manuscript

NIH-PA Author Manuscript

NIH-PA Author Manuscript

spins, *G(t)*, we evaluate the following equation in Matlab for several mixing times (*t*) ranging from 0–40 msec (1 msec intervals):

$$G(t) = Trace\left(S_{1x}e^{-iHt}S_{2x}e^{iHt}\right) \quad (2)$$

PMPT and CRDSD experiments were simulated by varying the ^{1}H spin-lock field strength (ω_I) from 0–70 kHz (in 2.5 kHz intervals) for each of three ^{15}N spin-lock fields (ω_S = 17.5, 33, and 50 kHz). Note that for the simulation of the CRDSD experiment, $\omega_I = 0$. The complete Hamiltonian in Eq. 1 was used in Eq. 2, with no motional processes or relaxation accounted for in the simulation.

Results

Spin Diffusion Between ^{15}N/^{15}N Distances in NAL and NAVL

The single crystals of NAL and NAVL were placed at an arbitrary orientation and kept in this position for all of the measurements. The nearest distance between ^{15}N nuclei in NAVL and NAL are 3.3 and 6.5 Å, which are good mimics of i, i+1 and i, i+4 ^{15}N/^{15}N distances in an ideal α-helix (~3 and ~6 Å). Both NAL and NAVL gave four unique ^{15}N resonances, therefore allowing for 12 total cross-peaks in each homonuclear 2D ^{15}N/^{15}N correlation spectrum. Figure 2 shows the results from 2D spectra acquired using PDSD, CRDSD and PMPT experiments. The noise floor in Figures 2 (NAL) and 3 (NAVL) is the same for all three spectra, so the cross-peak intensities for the three pulse sequences can be directly compared. For NAL, the PDSD experiment was found to be the most inefficient, with very weak cross-peaks. In contrast, the CRDSD and PMPT experiments both were quite efficient for long ^{15}N/^{15}N distances found within NAL, resulting in observation of all cross-peaks. This result supports previous experiments in which ^{15}N/^{15}N distances up to 8.5 Å were detected.[38, 49] For the NAVL crystal, the PDSD experiment gave significantly more intense cross-peaks than the NAL crystal. In fact, the intensities were larger than those detected using either the CRDSD or PMPT experiment. In the following sections, we compare the three experiments systematically, adjusting the experimental parameters that need to be optimized for strong cross-peaks in ^{15}N/^{15}N (or ^{13}C/^{13}C) correlation spectra for both short and long distances in oriented molecules (e.g., mixing times and spinlock field strengths). All of the intensity units for experiments conducted on NAL and NAVL have been normalized to make the intensities directly comparable between the PDSD, CRDSD, and PMPT experiments (i.e., same noise floor).

Note that another spin diffusion experiment referred to as CHHC or NHHN has shown to be quite useful in MAS solid-state NMR experiments.[50] While we were able to observe ^{15}N/^{15}N cross-peaks in NAL using NHHN, the signal to noise was only a fraction of that observed with the other experiments, and we therefore did not further pursue this pulse sequence as a viable alternative to PDSD, CRDSD or PMPT for oriented systems. Proton-proton mixing has, however, been shown to be useful in some oriented solid-state NMR experiments.[51]

Proton Driven Spin Diffusion

The PDSD experiment has been reported to be too inefficient as a transfer mechanism for detecting ^{15}N/^{15}N correlations in proteins.[37] This is expected due to the dependence of the spin diffusion probability (Ω) on the dipolar coupling strength between the two nuclei (ω_{ij}), given by Fermi's golden rule.[36, 52]:

NIH-PA Author Manuscript

NIH-PA Author Manuscript

NIH-PA Author Manuscript

$$\Omega=\frac{1}{2}\pi F_{ij}(0)\,\omega_{ij}^{2}t \tag{3}$$

$F_{ij}(0)$ is the zero-quantum lineshape and t is the time for spin diffusion to take place. Since the dipolar coupling is proportional to r_{ij}^{-3} (r is the distance between nuclei), the probability for a transition between two ^{15}N nuclei is quite small for r_{ij} > 6.5 Å and t < 5 sec (i.e., ^{15}N/^{15}N dipolar couplings < 4.5 Hz). For the NAL crystal, where the nearest ^{15}N/^{15}N distances are 6.5, 6.7, and 8.5 Å, the build-up of magnetization as a function of mixing time is highly inefficient (Figure 4 and Supplementary Figure 15). At a mixing time of 30 sec, the cross-peak displaying the most efficient transfer rate (cross-peak intensity divided by diagonal peak intensity) approaches only 20% (Supplementary Figure 15), echoing the spin diffusion probability expected from Fermi's golden rule.

For the NAVL single crystal, the results (Figure 5 and Supplementary Figure 16) agree well with the theoretical ω_{ij}^{2} dependence in Eq. 3, showing an efficient transfer of magnetization for intramolecular ^{15}N sites (a/c and b/d) and a substantially more inefficient transfer for intermolecular ^{15}N nuclei. Due to the shorter intra-molecular distance between ^{15}N spins of 3.3 Å (^{15}N/^{15}N dipolar couplings < 35 Hz),45 the magnetization was almost completely transferred at ~10 sec with ~50% efficiency at ~3–4 sec (Supplementary Figure 16). In contrast, at mixing times of 20 sec the transfer efficiency is only 40% between intermolecular sites, indicating that the PDSD has a clear distance dependence consistent with Fermi's golden rule. While a mixing time of 5–10 sec is somewhat long, the relaxation in the PDSD experiment is dominated by T_1, which is very long for ^{15}N magnetization, leading to strong cross-peaks in NAVL.

Cross-Relaxation Driven Spin Diffusion

The CRDSD mechanism has been reported to be a highly efficient mechanism of transferring magnetization in the NAVL crystal.37 Unlike the PDSD experiment (Figure 1), there are two variables that need to be independently optimized to achieve the most favorable transfer: 1) the ^{15}N spinlock field strength and 2) the mixing time. Figure 6 shows changes in the cross-peak intensities in NAL upon variation of the ^{15}N spinlock field for a 10 msec mixing time. Due to relaxation during the spinlock (from multiple relaxation channels), we plot the absolute intensity of the cross-peaks rather than the normalized cross-peak intensity.53, 54 The maximum intensity of all cross-peaks occurs for $\omega_s/2\pi$ = 17–22 kHz (Figure 6). A similar range was found to give maximal cross-peak heights in the NAVL dipeptide crystal,37 which is in quantitative agreement with our measurements (Figure 7).

We also performed a systematic build-up of the NAL and NAVL cross-peaks by varying the mixing time at a fixed ^{15}N spinlock field of 21 kHz. From the series of 2D spectra acquired at different mixing times, it is apparent that the magnetization has reached a maximum for all NAL cross-peaks between 5–15 msec (Figure 8). Therefore, the magnetization transfer is much more efficient in the CRDSD than the PDSD experiment. In Figure 9, we plot the cross-peak intensities as a function of the mixing time from the NAVL sample, which are consistent with those previously reported37 (even the crystal orientation is similar). The results obtained for NAL and NAVL suggest that both intra- and inter-molecular magnetization transfers proceed essentially at the same rate (Figures 8 and 9). Since the internuclear distances in the crystals are strikingly different, 3.3 vs. 6.5 Å, there is a potential problem for using these experiments to sequentially assign resonances. Ideally, for a *walk* through the backbone ^{15}N residues (i.e., sequential resonance assignment) one would only want to correlate residue i with the adjacent i±1. Due to the tightly coupled proton network, the CRDSD mechanism, while relying on the presence of direct ^{15}N/^{15}N

NIH-PA Author Manuscript

NIH-PA Author Manuscript

NIH-PA Author Manuscript

couplings, reduces and/or in some cases essentially removes the distance dependence of the cross-peak intensities.

Proton-Mediated Proton Transfer Mechanism

Unlike the PDSD and CRDSD pulse schemes, there are three experimental parameters that need to be optimized for the PMPT experiment: 1) ^{15}N spinlock, 2) ^{1}H spinlock (mismatch condition), and 3) the mixing time. It is noted that the PMPT experiment is essentially the oriented solid-state NMR version of the proton assisted recoupling (PAR) experiment used in MAS experiments.41⁻43

For our analysis of PMPT, we first set the mixing time to 10 msec, and adjusted the ^{1}H spinlock field at three different ^{15}N spinlock values (ω_S = 21, 37.5, and 52.5 kHz). Figure 10 shows the experimental results for NAL. The PMPT mechanism has previously been reported to be most efficient in NAL when the ^{1}H RF field is mismatched by 110% from that of the ^{15}N spinlock.38, 49 When the ^{1}H spinlock approaches the Hartmann-Hahn match,55 part of the magnetization is transferred back to the protons, depleting the observable ^{15}N magnetization. Therefore, there is a trade-off between the efficiency of the proton-mediated transfer mechanism and the Hartmann-Hahn match. Figure 10 shows the cross-peak intensities as a function of the ^{1}H spinlock field. We found that two of the curves (^{15}N spinlocks of 37.5 and 52.5 kHz) each have two relative maxima that are located above and below the Hartmann-Hahn match. For the 21 kHz ^{15}N spinlock curve, there is only one maximum, which is present above the Hartmann-Hahn matching condition (32 kHz ^{1}H spinlock or 155% of the ^{15}N spinlock value). Interestingly, we found that the absolute cross-peak intensities were actually higher at a lower ^{15}N spinlock value (and therefore ^{1}H spinlock field) for a mixing time of 10 msec. To further investigate this, we performed a systematic build-up of the mixing time for the three ^{15}N spinlock values and the optimized ^{1}H mismatch values determined from Figure 10. As with the CRDSD mechanism, all of the cross-peaks were observed with a maximum intensity reached at 5–10 msec (see Figure 11). As suggested by the data in Figure 10, the ^{15}N spinlock at the lowest value of 21 kHz gave the most intense cross-peaks (Figure 11). Therefore, this suggests that the mechanism is a combination of both direct ^{15}N/^{15}N couplings (the CRDSD mechanism), as well as the proton-mediated effect (PMPT mechanism).

We repeated the PMPT experiments using NAVL. We found that the most efficient transfer for intramolecular ^{15}N nuclei was due to the 3 sec Z-filter element used in the pulse sequence (see Figure 1). In fact, the removal of the MMHH element from the PMPT experiment makes the pulse sequence identical to the PDSD experiment, which was shown to give strong intramolecular cross-peaks in 3 sec for NAVL (Figure 3). Finally, we analyzed the cross-peak build-up at a ^{15}N spinlock field of 57.5 kHz as a function of the ^{1}H spinlock field. The cross-peak intensity profiles for intermolecular ^{15}N/^{15}N correlations are nearly identical to those found in NAL (compare intermolecular cross-peaks ad in Figures 10 and 12). However, for intramolecular ^{15}N/^{15}N transfer, the MMHH condition decreased the cross-peak intensity (Figure 12). The dotted line in Figure 12 indicates the most optimal ^{1}H spinlock field for the PMPT mechanism, and this does not give the maximum intensity for the intramolecular^{15}N/^{15}N peak ad, indicating the PMPT mechanism only depleted the signal by the transfer of magnetization to ^{1}H (i.e., the Hartmann-Hahn mechanism). These results suggest a more efficient transfer between short distances from using the PDSD experiment rather than either PMPT or CRDSD.

Simulations

To validate the results above, we performed numerical simulations of the PMPT and CRDSD experiments for NAL. The DC values used in the simulations were obtained by

NIH-PA Author Manuscript

NIH-PA Author Manuscript

NIH-PA Author Manuscript

rotating the NAL crystal coordinates to maximize the agreement with the experimental DCs and CSs measured from a PISEMA experiment. The principal values for the ^{15}N chemical shift tensor were δ_{11}=64, δ_{22}=77, and δ_{33}=217 ppm.56 From this crystal orientation, we calculated all relevant angles relative to the magnetic field, and therefore all dipolar coupling frequencies (b_{ij} and d_{ij} from Eq. 1; Supplementary Table I).

The results from the simulation are reported in Figure 13. We set the ^{15}N spinlock field at values similar to those used in the experiments on NAL (17, 33, and 50 kHz). The ^{1}H spinlock field was varied from 0–70 kHz, and the time of the transfer from 0–40 msec. In Figure 13A, the transfer efficiencies are plotted as a function of the ^{1}H spinlock at a mixing time of 20 msec. The simulations at three different spinlock fields clearly show that at a small ^{15}N spinlock value, the magnetization transfer is more efficient than those obtained at larger spinlock fields. Additionally, the CRDSD experiment (^{1}H spinlock = 0 kHz) is reproduced by the simulations: a smaller ^{15}N spinlock of 17.5 kHz gives efficient transfer, while larger ^{15}N spinlock fields (33, 50 kHz; RFDSD experiment) result in little or no transfer.37, 47 The reason for this observation is that a low ^{15}N spin-lock field (17 kHz) is unable to completely decouple ^{15}N nuclei from ^{1}H, whereas, a larger spin-lock field does sufficiently decouple the heteronuclear dipolar coupling.

For the PMPT experiment, the HHMM fields that give optimal transfer are 29, 21, and 10% for ^{15}N spinlocks of 17.5, 33, and 50 kHz, respectively, which is in good agreement with the experimental values of 55, 27, and 19% for NAL. The small deviations from experiment can be accounted for by offset dependencies at smaller spin-lock fields, small errors in the calculation of the experimental spinlock fields, and the approximation of only 12 spins in the simulation. The simulations also show that the transfer efficiencies plotted as a function of the mixing time were in close agreement with those found experimentally. At ~10 msec the transfer efficiencies (Figure 13B) in the simulation reached a maximum, which agrees closely with those reported experimentally in Figures 8 and 11. Taken together, these simulations show that the magnetization in NAL (long distances) is more efficiently transferred with PMPT and CRDSD than PDSD.

Discussion

In this work, we present a comparison of the spin diffusion experiments currently available for oriented solid-state NMR experiments. While SLF experiments are the most reliable method to directly probe anisotropic structural restraints (DC and CS), no definitive sequential assignment schemes are currently used to accurately and efficiently assign the spectra.

In pursuit of an assignment strategy, we compared the efficiencies of three spin diffusion methods with model compounds that are mimics of short and long range distances in proteins (NAL and NAVL). In addition, the ability to detect long-range connectivities in proteins will be important for implementing structural restraints. In order to directly compare the intensities observed for NAL between the PDSD (Figure 4), CRDSD (Figure 8), and PDSD (Figure 11) experiments, we need to normalize the PDSD data to account for the increased experimental data acquisition time due to the mixing period. The results are plotted in Figure 14 (values in Table I), and show that the PMPT experiment carried out with low spinlock fields (^{1}H 32.5 kHz, ^{15}N 21 kHz) gives on average a factor of 34 greater intensity per unit time than PDSD (30 sec mixing time) and a factor of 1.4 more signal than the CRDSD experiment. Therefore, both the CRDSD and PMPT experiments are highly efficient mechanisms for transferring magnetization at distances up to 8 Å with modest spinlock fields (17–30 kHz) and mixing times (~10 msec). For the PMPT experiment, we found that the mismatched Hartmann-Hahn condition is most efficient in transferring

NIH-PA Author Manuscript

NIH-PA Author Manuscript

NIH-PA Author Manuscript

magnetization at weaker spinlock fields for ^{1}H and ^{15}N (Figure 14 and Table I). The latter is an important point, since it is always preferable to use lower powers in experiments to minimize the stress to NMR hardware. While the probes have improved to handle large spinlock fields (approaching 100 kHz) for 20 msec under low electric field conditions,[46, 57] sample heating still occurs, which is more pronounced at high magnetic fields.

From the prospective of the sequential resonance assignment in SLF experiments such as PISEMA, HIMSELF or SAMPI4 the most useful $^{15}N/^{15}N$ correlations are i, i+1. This will make the assignments unambiguous and directly amenable to implementing DC and CS restraints in calculating membrane protein structure and topology. A direct comparison of the cross-peak intensity observed for PDSD, CRDSD, and PMPT is observed in Figures 5, 9, and 12, respectively. As for NAL, we calculated the normalized intensity per unit time, with the results shown in Figure 14 (values in Table I). We find that on average, PDSD with a 4 sec mixing time results in the most signal. It gives a factor of 3.5 more signal than the PMPT experiment and a factor of 7 more signal than the CRDSD experiment. Importantly, unlike PDSD, the CRDSD and PMPT sequences essentially erase the distance dependence, making all $^{15}N/^{15}N$ correlations from 3.3 to 8 Å observable with similar cross-peak intensity. In fact, we found that the PMPT experiment with a 3 sec Z-filter element (acting like a PDSD experiment) significantly reduced cross-peak intensities observed between intramolecular ^{15}N nuclei spaced 3.3 Å apart. Although this might be attractive for long-range distances (e.g., i, i+4 distances), it is likely to be problematic for resonance assignments. Recently, a paper by Nevzorov and co-workers introduced the PMPT scheme for assigning membrane proteins. While this method is very promising for measuring long-range distances, the observation of correlations other than i, i+1, makes this scheme cumbersome for assignment purposes.[44]

A final consideration is that spinlock experiments such as CRDSD and PMPT result in magnetization that decays with $T_{1\rho}$ (from multiple relaxation channels), whereas the magnetization in the PDSD experiment decays with T_1. Since T_1 in solids is relatively long for ^{15}N spins, the PDSD experiment still might be the most sensitive experiment available for unambiguous resonance assignment of membrane proteins (i.e., correlating only i, i+1 resonances). Since its first application in oriented experiments on glass plates, there have been no reported uses of this pulse sequence for assignment purposes, presumably due to the significant inhomogenous line-broadening present in the spectra, leading to poor signal to noise. Bicelle technology will likely allow these experiments to be usable for sequential assignment (PDSD) and long-range distance restraints (CRDSD and PMPT).[44]

Supplementary Material

Refer to Web version on PubMed Central for supplementary material.

Acknowledgments

This work was supported by the National Institutes of Health (Grants GM64742, HL80081, and GM072701 to G.V.). We thank Professor Alex Nevzorov for helpful comments concerning our manuscript and for exciting discussions about the assignment process. We are also grateful to Dr. Dan Mullen for synthesizing NAVL.

References

(1). Naito A. Structure Elucidation of Membrane-Associated Peptides and Proteins in Oriented Bilayers by Solid-State NMR Spectroscopy. Solid State Nucl. Magn. Reson. 2009; 36:67–76. [PubMed: 19647984]

NIH-PA Author Manuscript

NIH-PA Author Manuscript

NIH-PA Author Manuscript

(2). De Angelis AA, Howell SC, Nevzorov AA, Opella SJ. Structure Determination of a Membrane Protein with Two Trans-Membrane Helices in Aligned Phospholipid Bicelles by Solid-State NMR Spectroscopy. J. Am. Chem. Soc. 2006; 128:12256–12267. [PubMed: 16967977]

(3). Park SH, Mrse AA, Nevzorov AA, Mesleh MF, Oblatt-Montal M, Montal M, Opella SJ, Valentine KG, Mesleh MF, Opella SJ, Ikura M, Ames JB. Three-Dimensional Structure of the Channel-Forming Trans-Membrane Domain of Virus Protein “u” (Vpu) from HIV-1 Structure, Topology, and Dynamics of Myristoylated Recoverin Bound to Phospholipid Bilayers. J Mol Biol. 2003; 333:409–24. [PubMed: 14529626]

(4). Li C, Yi M, Hu J, Zhou HX, Cross TA. Solid-State NMR and MD Simulations of the Antiviral Drug Amantadine Solubilized in DMPC Bilayers. Biophys. J. 2008; 94:1295–1302. [PubMed: 17890391]

(5). Durr UH, Yamamoto K, Im SC, Waskell L, Ramamoorthy A. Solid-State NMR Reveals Structural and Dynamical Properties of a Membrane-Anchored Electron-Carrier Protein, Cytochrome b5. J. Am. Chem. Soc. 2007; 129:6670–6671. [PubMed: 17488074]

(6). Henzler Wildman KA, Lee DK, Ramamoorthy A. Mechanism of Lipid Bilayer Disruption by the Human Antimicrobial Peptide, LL-37. Biochemistry. 2003; 42:6545–6558. [PubMed: 12767238]

(7). Traaseth NJ, Shi L, Verardi R, Mullen D, Barany G, Veglia G. Determination of Membrane Protein Structure and Topology using a Hybrid Solution and Solid-State NMR Approach. Proc Natl Acad Sci. 2009; 106:10165–70. [PubMed: 19509339]

(8). Traaseth NJ, Ha KN, Verardi R, Shi L, Buffy JJ, Masterson LR, Veglia G. Structural and Dynamic Basis of Phospholamban and Sarcolipin Inhibition of Ca(2+)-ATPase. Biochemistry. 2008; 47:3–13. [PubMed: 18081313]

(9). Buffy JJ, Traaseth NJ, Mascioni A, Gor'kov PL, Chekmenev EY, Brey WW, Veglia G. Two-Dimensional Solid-State NMR Reveals Two Topologies of Sarcolipin in Oriented Lipid Bilayers. Biochemistry. 2006; 45:10939–10946. [PubMed: 16953579]

(10). Fu R, Gordon ED, Hibbard DJ, Cotten M. High Resolution Heteronuclear Correlation NMR Spectroscopy of an Antimicrobial Peptide in Aligned Lipid Bilayers: Peptide-Water Interactions at the Water-Bilayer Interface. J. Am. Chem. Soc. 2009; 131:10830–10831. [PubMed: 19621928]

(11). Sau SP, Ramanathan KV. Visualization of Enantiomers in the Liquid-Crystalline Phase of a Fragmented DNA Solution. J Phys Chem B. 2009; 113:1530–1532. [PubMed: 19133792]

(12). Wu CH, Ramamoorthy A, Opella SJ. High-Resolution Heteronuclear Dipolar Solid-State NMR Spectroscopy. J Mag Res. 1994; 109:270–272.

(13). Yamamoto K, Lee DK, Ramamoorthy A. Broadband-PISEMA Solid-State NMR Spectroscopy. Chem Phys Lett. 2005; 407:289–93.

(14). Nevzorov AA, Opella SJ. Selective Averaging for High-Resolution Solid-State NMR Spectroscopy of Aligned Samples. J. Magn. Reson. 2007; 185:59–70. [PubMed: 17074522]

(15). Dvinskikh SV, Yamamoto K, Ramamoorthy A. Heteronuclear Isotropic Mixing Separated Local Field NMR Spectroscopy. J. Chem. Phys. 2006; 125:34507. [PubMed: 16863362]

(16). Gopinath T, Veglia G. Sensitivity Enhancement in Static Solid-State NMR Experiments Via Single- and Multiple-Quantum Dipolar Coherences. J. Am. Chem. Soc. 2009; 131:5754–5756. [PubMed: 19351170]

(17). Gopinath T, Verardi R, Traaseth NJ, Veglia G. Sensitivity Enhancement of Separated Local Field Experiments: Application to Membrane Proteins. J Phys Chem B. 2010; 114:5089–5095. [PubMed: 20349983]

(18). Gopinath T, Traaseth NJ, Mote K, Veglia G. Sensitivity Enhanced Heteronuclear Correlation Spectroscopy in Multidimensional Solid-State NMR of Oriented Systems Via Chemical Shift Coherences. J. Am. Chem. Soc. 2010; 132:5357–5363. [PubMed: 20345172]

(19). Nevzorov AA, Opella SJ. Structural Fitting of PISEMA Spectra of Aligned Proteins. J. Magn. Reson. 2003; 160:33–39. [PubMed: 12565046]

(20). Bertram R, Asbury T, Fabiola F, Quine JR, Cross TA, Chapman MS. Atomic Refinement with Correlated Solid-State NMR Restraints. J. Magn. Reson. 2003; 163:300–309. [PubMed: 12914845]

NIH-PA Author Manuscript

NIH-PA Author Manuscript

NIH-PA Author Manuscript

(21). Shi L, Traaseth NJ, Verardi R, Cembran A, Gao J, Veglia G. A Refinement Protocol to Determine the Structure, Topology, and Depth of Insertion of Membrane Proteins using Hybrid Solution and Solid-State Restraints. J Biomolec NMR. 2009; 44:195–205.

(22). Marassi FM, Opella SJ. A Solid-State NMR Index of Helical Membrane Protein Structure and Topology. J Magn Reson. 2000; 144:150–5. [PubMed: 10783285]

(23). Wang J, Denny J, Tian C, Kim S, Mo Y, Kovacs F, Song Z, Nishimura K, Gan Z, Fu R, Quine JR, Cross TA. Imaging Membrane Protein Helical Wheels. J. Magn. Reson. 2000; 144:162–167. [PubMed: 10783287]

(24). Mesleh MF, Lee S, Veglia G, Thiriot DS, Marassi FM, Opella SJ. Dipolar Waves Map the Structure and Topology of Helices in Membrane Proteins. J Am Chem Soc. 2003; 125:8928–35. [PubMed: 12862490]

(25). Mascioni A, Veglia G. Theoretical Analysis of Residual Dipolar Coupling Patterns in Regular Secondary Structures of Proteins. J. Am. Chem. Soc. 2003; 125:12520–12526. [PubMed: 14531696]

(26). Page RC, Kim S, Cross TA. Transmembrane Helix Uniformity Examined by Spectral Mapping of Torsion Angles. Structure. 2008; 16:787–797. [PubMed: 18462683]

(27). Vosegaard T, Nielsen NC. Towards High-Resolution Solid-State NMR on Large Uniformly 15N- and [13C,15N]-Labeled Membrane Proteins in Oriented Lipid Bilayers. J. Biomol. NMR. 2002; 22:225–247. [PubMed: 11991353]

(28). Igumenova TI, Wand AJ, McDermott AE. Assignment of the Backbone Resonances for Microcrystalline Ubiquitin. J. Am. Chem. Soc. 2004; 126:5323–5331. [PubMed: 15099118]

(29). Reif B, Hohwy M, Jaroniec CP, Rienstra CM, Griffin RG. NH-NH Vector Correlation in Peptides by Solid-State NMR. J. Magn. Reson. 2000; 145:132–141. [PubMed: 10873504]

(30). Quine JR, Achuthan S, Asbury T, Bertram R, Chapman MS, Hu J, Cross TA. Intensity and Mosaic Spread Analysis from PISEMA Tensors in Solid-State NMR. J. Magn. Reson. 2006; 179:190–198. [PubMed: 16413215]

(31). Traaseth NJ, Buffy JJ, Zamoon J, Veglia G. Structural Dynamics and Topology of Phospholamban in Oriented Lipid Bilayers using Multidimensional Solid-State NMR. Biochemistry. 2006; 45:13827–13834. [PubMed: 17105201]

(32). Traaseth NJ, Verardi R, Torgersen KD, Karim CB, Thomas DD, Veglia G. Spectroscopic Validation of the Pentameric Structure of Phospholamban. Proc. Natl. Acad. Sci. U. S. A. 2007; 104:14676–14681. [PubMed: 17804809]

(33). Muller SD, De Angelis AA, Walther TH, Grage SL, Lange C, Opella SJ, Ulrich AS. Structural Characterization of the Pore Forming Protein TatAd of the Twin-Arginine Translocase in Membranes by Solid-State 15N-NMR. Biochim. Biophys. Acta. 2007; 1768:3071–3079. [PubMed: 17980349]

(34). De Angelis AA, Nevzorov AA, Park SH, Howell SC, Mrse AA, Opella SJ. High-Resolution NMR Spectroscopy of Membrane Proteins in Aligned Bicelles. J. Am. Chem. Soc. 2004; 126:15340–15341. [PubMed: 15563135]

(35). Szeverenyi NM, Sullivan MJ, Maciel GE. Observation of Spin Exchange by Two-Dimensional Fourier Transform 13C Cross Polarization-Magic-Angle Spinning. J. Magn. Reson. 1982; 47:462–75.

(36). Suter D, Ernst RR. Spin Diffusion in Resolved Solid-State NMR Spectra. Phys. Rev. B. 1985; 32:5608–27.

(37). Xu J, Struppe J, Ramamoorthy A. Two-Dimensional Homonuclear Chemical Shift Correlation Established by the Cross-Relaxation Driven Spin Diffusion in Solids. J. Chem. Phys. 2008; 128:052308. [PubMed: 18266425]

(38). Nevzorov AA. Mismatched Hartmann-Hahn Conditions Cause Proton-Mediated Intermolecular Magnetization Transfer between Dilute Low-Spin Nuclei in NMR of Static Solids. J. Am. Chem. Soc. 2008; 130:11282–11283. [PubMed: 18680251]

(39). Cross TA, Frey MH, Opella SJ. Nitrogen-15 Spin Exchange in a Protein. J Am Chem Soc. 1983; 105:7471–3.

NIH-PA Author Manuscript

NIH-PA Author Manuscript

NIH-PA Author Manuscript

(40). Marassi FM, Gesell JJ, Valente AP, Kim Y, Oblatt-Montal M, Montal M, Opella SJ. Dilute Spin-Exchange Assignment of Solid-State NMR Spectra of Oriented Proteins: Acetylcholine M2 in Bilayers. J. Biomol. NMR. 1999; 14:141–148. [PubMed: 10427741]

(41). Lewandowski JR, De Paepe G, Griffin RG. Proton Assisted Insensitive Nuclei Cross Polarization. J. Am. Chem. Soc. 2007; 129:728–729. [PubMed: 17243786]

(42). De Paepe G, Lewandowski JR, Loquet A, Bockmann A, Griffin RG. Proton Assisted Recoupling and Protein Structure Determination. J. Chem. Phys. 2008; 129:245101. [PubMed: 19123534]

(43). Lewandowski JR, De Paepe G, Eddy MT, Griffin RG. (15)N-(15)N Proton Assisted Recoupling in Magic Angle Spinning NMR. J. Am. Chem. Soc. 2009; 131:5769–5776. [PubMed: 19334788]

(44). Knox RW, Lu GJ, Opella SJ, Nevzorov AA. A Resonance Assignment Method for Oriented-Sample Solid-State NMR of Proteins. J. Am. Chem. Soc. 2010; 132:8255–8257. [PubMed: 20509649]

(45). Carroll PJ, Stewart PL, Opella SJ. Structures of Two Model Peptides: N-Acetyl-D,L-Valine and N-Acetyl-L-Valyl-L-Leucine. Acta Crystallogr. Sect. C. 1990; 46:243–6.

(46). Gor'kov PL, Chekmenev EY, Li C, Cotten M, Buffy JJ, Traaseth NJ, Veglia G, Brey WW. Using Low-E Resonators to Reduce RF Heating in Biological Samples for Static Solid-State NMR Up to 900 MHz. J. Magn. Reson. 2007; 185:77–93. [PubMed: 17174130]

(47). Robyr P, Meier BH, Ernst RR. Radio-Frequency-Driven Nuclear Spin Diffusion in Solids. Chem Phys Lett. 1989; 162:417–423.

(48). Robyr P, Gan Z. Radiofrequency-Driven and Slow-Magic-Angle-Sample-Spinning Polarization-Transfer Techniques: A Comparative Study. J. Magn. Reson. 1998; 131:254–260. [PubMed: 9571101]

(49). Nevzorov AA. High-Resolution Local Field Spectroscopy with Internuclear Correlations. J. Magn. Reson. 2009; 201:111–114. [PubMed: 19733109]

(50). Lange A, Luca S, Baldus M. Structural Constraints from Proton-Mediated Rare-Spin Correlation Spectroscopy in Rotating Solids. J. Am. Chem. Soc. 2002; 124:9704–9705. [PubMed: 12175218]

(51). Ramamoorthy A, Gierasch LM, Opella SJ. Three-Dimensional Solid-State NMR Correlation Experiment with 1H Homonuclear Spin Exchange. J. Magn. Reson. B. 1996; 111:81–84. [PubMed: 8620287]

(52). Bronniman CE, Szeverenyi NM, Maciel GE. 13C Spin Diffusion of Adamantane. J. Chem. Phys. 1983; 79:3694–700.

(53). deAzevedo ER, Bonagamba TJ, Schmidt-Rohr K. Pure-Exchange Solid-State NMR. J Magn Reson. 2000; 142:86–96. [PubMed: 10617438]

(54). Vosegaard T, Nielsen NC. Improved Pulse Sequences for Pure Exchange Solid-State NMR Spectroscopy. Magn Reson Chem. 2004; 42:285–290. [PubMed: 14745809]

(55). Hartmann SR, Hahn EL. Phys Rev. 1962; 128:2042–2053.

(56). Wu CH, Ramamoorthy A, Gierasch LM, Opella SJ. Simultaneous Characterization of the Amide 1H Chemical Shift, 1H-15N Dipolar, and 15N Chemical Shift Interaction Tensors in a Peptide Bond by Three-Dimensional Solid-State NMR Spectroscopy. J Am Chem Soc. 1995; 117:6148–6149.

(57). Stringer JA, Bronnimann CE, Mullen CG, Zhou DH, Stellfox SA, Li Y, Williams EH, Rienstra CM. Reduction of RF-Induced Sample Heating with a Scroll Coil Resonator Structure for Solid-State NMR Probes. J. Magn. Reson. 2005; 173:40–48. [PubMed: 15705511]

NIH-PA Author Manuscript

NIH-PA Author Manuscript

NIH-PA Author Manuscript

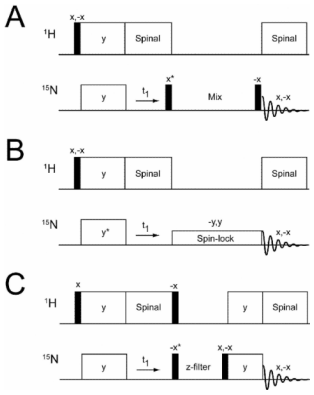

FIGURE 1.

Pulse sequences used to correlate $^{15}N/^{15}N$: A) proton driven spin diffusion (PDSD), B) cross-relaxation driven spin diffusion (CRDSD), and C) proton-mediated proton transfer (PMPT). Asterisks indicate pulses that were adjusted by 90° to acquire phase-sensitive data in the indirect dimension (ω1).

NIH-PA Author Manuscript

NIH-PA Author Manuscript

NIH-PA Author Manuscript

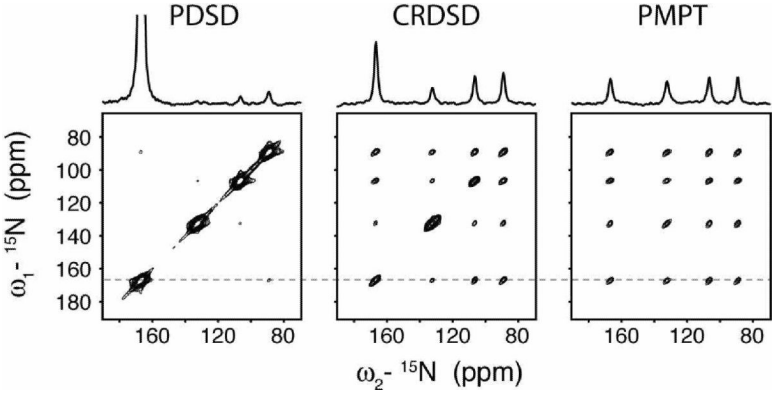

FIGURE 2.

Comparison of spin diffusion experiments on NAL. Note that the peak naming convention (peaks *a*, *b*, *c*, *d*) is from the most downfield (peak *a*) to the most upfield (peak *d*). For example, the cross-peak at ω_2 = 167 ppm and ω_1 = 133 ppm is referred to as *ab*. The PDSD experiment utilized a 3 sec mixing time, the CRDSD experiment used a ^{15}N spinlock field of 21 kHz, and the PMPT experiment used a Z-filter of 3 sec and ^{1}H and ^{15}N spinlock fields of 30 kHz and 21 kHz, respectively. The CRDSD and PMPT experiment used a mixing time of 10 msec. 1D sections are taken from the dotted line in the 2D spectra. All 2D spectra are shown at the same contour level, allowing for a direct comparison of peak intensities.

NIH-PA Author Manuscript

NIH-PA Author Manuscript

NIH-PA Author Manuscript

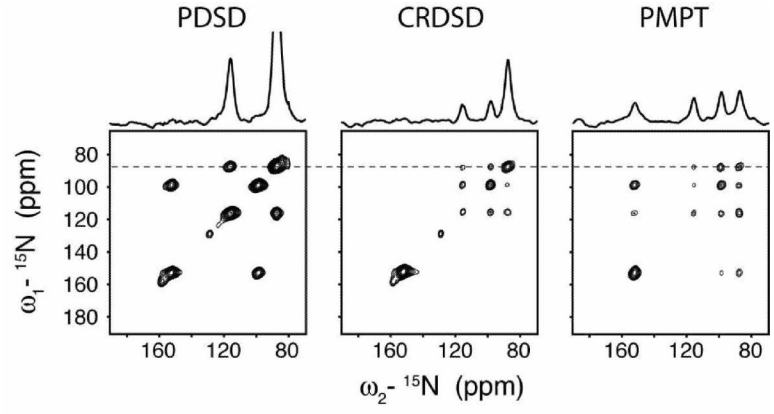

FIGURE 3.

Comparison of spin diffusion experiments on NAVL. Note that the peak naming convention (peaks *a*, *b*, *c*, *d*) is from the most downfield (peak *a*) to the most upfield (peak *d*). For example, the cross-peak at ω_2 = 152 ppm and ω_1 = 99 ppm is referred to as *ac*. The PDSD experiment utilized a 3 sec mixing time, the CRDSD experiment used a ^{15}N spinlock field of 21 kHz, and the PMPT experiment used a Z-filter of 3 sec and ^{1}H and ^{15}N spinlock fields of 65 kHz and 55 kHz, respectively. The CRDSD and PMPT experiment used a mixing time of 10 msec. 1D sections are taken from the dotted line in the 2D spectra. All 2D spectra are shown at the same contour level, allowing for a direct comparison of peak intensities.

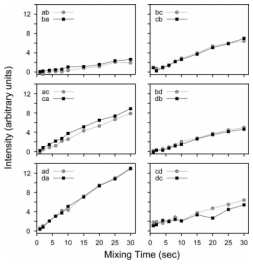

FIGURE 4.

PDSD experiments on the NAL single crystal. All 12 cross-peaks are shown from the spectra are shown in arbitrary intensity units. All experiments from the NAL crystal (Figures 6, 8, 10 and 11) are shown in the same relative units (i.e., same noise floor).

NIH-PA Author Manuscript
NIH-PA Author Manuscript
NIH-PA Author Manuscript

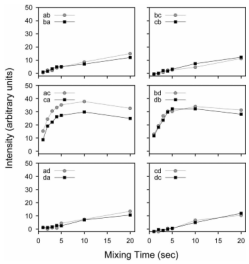

FIGURE 5.

PDSD experiments on the NAVL single crystal. All 12 cross-peaks are shown from the spectra are shown in arbitrary intensity units. All experiments from the NAVL crystal (Figures 7, 9 and 12) are shown in the same relative units (i.e., same noise floor).

NIH-PA Author Manuscript
NIH-PA Author Manuscript
NIH-PA Author Manuscript

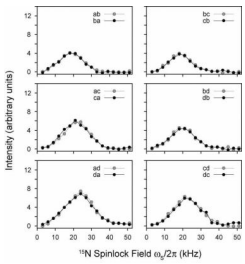

FIGURE 6.

CRDSD experiments on the NAL single crystal. The ^{15}N spinlock field was varied while keeping the mixing time fixed at 10 msec. The intensities are expressed in arbitrary units. All experiments were acquired in an interleaved manner to avoid potential differences in the experiments, and are therefore relevant to compare within each figure.

NIH-PA Author Manuscript NIH-PA Author Manuscript NIH-PA Author Manuscript

NIH-PA Author Manuscript

NIH-PA Author Manuscript

NIH-PA Author Manuscript

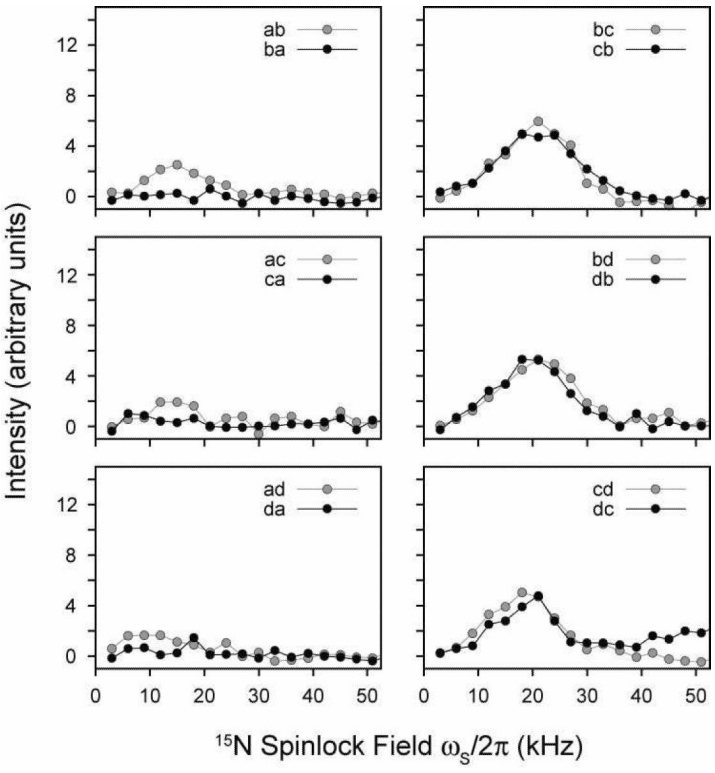

FIGURE 7.

CRDSD experiments on the NAVL single crystal. The ^{15}N spinlock field was varied while keeping the mixing time fixed at 10 msec. The intensities are expressed in arbitrary units.

NIH-PA Author Manuscript
NIH-PA Author Manuscript
NIH-PA Author Manuscript

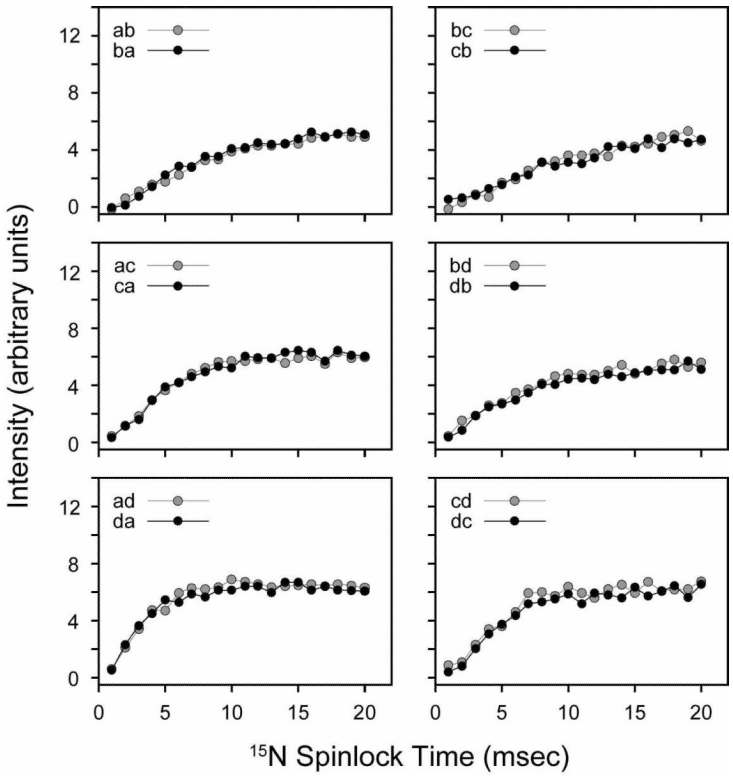

FIGURE 8.

CRDSD experiments on the NAL single crystal. The ^{15}N spinlock field was fixed at 21 kHz, while the mixing time was varied between 1–20 msec. The cross-peak intensities are plotted in arbitrary units.

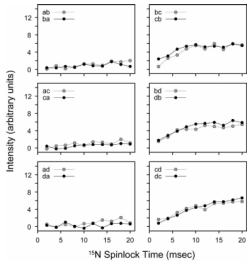

FIGURE 9.

CRDSD experiments on the NAVL single crystal. The ^{15}N spinlock field was fixed at 21 kHz, while the mixing time was varied between 1–20 msec. The cross-peak intensities are plotted in arbitrary units.

NIH-PA Author Manuscript
NIH-PA Author Manuscript
NIH-PA Author Manuscript

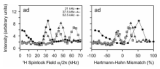

FIGURE 10.

PMPT experiments on the NAL single crystal. The ^{1}H spinlock field was varied between 0–70 kHz for three different ^{15}N spinlock fields (21, 37.5, and 52.5 kHz). The values are also plotted as the Hartmann-Hahn mismatch percentage. The mixing time was fixed at 10 msec for all points. Cross-peak intensities are plotted in arbitrary units. The dip in the curves is due to the Hartmann-Hahn match. The other cross-peaks are essentially the same as that plotted for the cross-peak ad. All other curves are shown in Supplementary Figures 17 and 18.

NIH-PA Author Manuscript
NIH-PA Author Manuscript
NIH-PA Author Manuscript

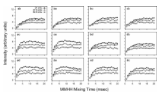

FIGURE 11.

PMPT experiments on the NAL single crystal. The ^{1}H spinlock field was set to 32.5, 47.5 and 62.5 kHz for 21, 37.5 and 52.5 kHz ^{15}N spinlock, respectively, based on the results shown in Figure 10. The mismatched Hartmann-Hahn (MMHH) mixing time was varied from 1–20 msec. The cross-peak intensities are in arbitrary units (i.e., not divided by the diagonal peak intensity).

NIH-PA Author Manuscript
NIH-PA Author Manuscript
NIH-PA Author Manuscript

NIH-PA Author Manuscript

NIH-PA Author Manuscript

NIH-PA Author Manuscript

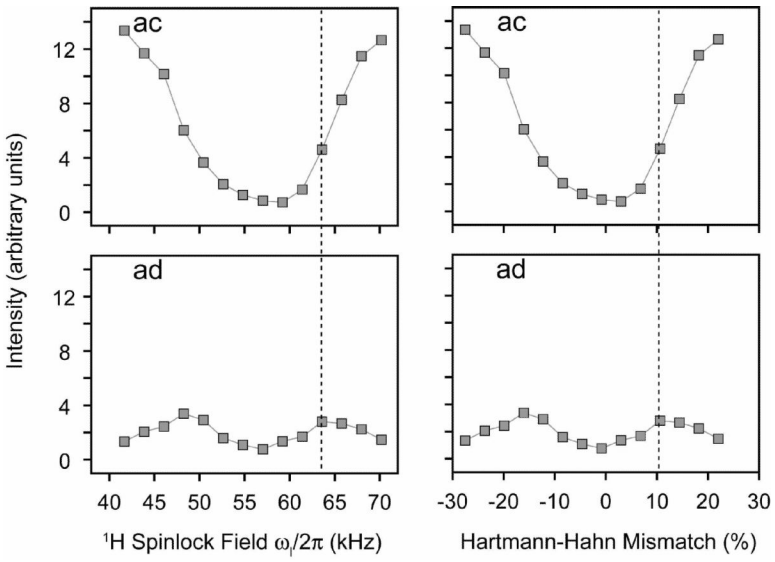

FIGURE 12.

PMPT experiments on the NAVL single crystal. The ^{1}H spinlock field was varied for a ^{15}N spinlock of 57.5 kHz. The mixing time was fixed at 10 msec for all points. The curves plotted are for crosspeaks ac (intramolecular $^{15}N/^{15}N$, 3.3 Å) and ad (intermolecular $^{15}N/^{15}N$, > 6 Å). Intensities are plotted in arbitrary units. The dip in the curves is due to the Hartmann-Hahn match. The dotted line indicates the best transfer ^{1}H spinlock value for intermolecular transfer in NAVL. The optimal value for intermolecular transfer results in less magnetization transfer for intramolecular sites. The other cross-peaks are essentially the same as those plotted for the cross-peaks ac and ad. All other curves are shown in Supplementary Figures 18 and 19.

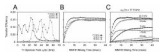

FIGURE 13.

Twelve-spin simulations of the PMPT and CRDSD experiments on the NAL single crystal. A) Varying the spinlock field on the ^{1}H spinlock field for three different ^{15}N spinlock fields (17.5, 33, and 50 kHz) at a MMHH mixing time of 20 msec. Note that for a ^{1}H spinlock field of 0 kHz, this is the CRDSD experiment for a 17.5 kHz ^{15}N spin-lock and the RFDSD experiment for larger ^{15}N spin-locks. B) Build-up for the most optimal transfer efficiencies in panel A. For ^{15}N spinlocks of 17.5, 33, and 50 kHz, the ^{1}H spinlock field was maximal at 22.5, 40, and 55 kHz, respectively. C) Several mixing time build-up curves for different ^{1}H spinlock fields when the ^{15}N spinlock was set to 17.5 kHz.

NIH-PA Author Manuscript
NIH-PA Author Manuscript
NIH-PA Author Manuscript

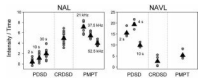

Figure 14.

Comparison of PDSD, CRDSD, and PMPT experiments for NAL and NAVL normalized for the mixing time in the PDSD experiment. Since a 3 sec recycle delay was used for every experiment, normalization was done by dividing the PDSD 2D peak intensities by 1.29, 1.53, 2.08, and 3.32 to account for 2, 4, 10, and 30 sec mixing times, respectively. Although the PMPT experiment used a 3 sec Z-filter time, no normalization was done for this experiment due to the fact that a much shorter time can be used that would only marginally influence the experimental acquisition time.44 For NAVL, much of the magnetization created in the PMPT experiment originated from the 3 sec Z-filter time. Circles represent all cross peaks observed in the NAL spectra and only intramolecular $^{15}N/^{15}N$ cross-peaks in the NAVL crystal (i.e., peaks ac, ca, bd, and db). Triangles represent the average of the cross-peak intensities shown (values in Table I). The CRDSD experimental cross-peaks are from the spectra using a 10 msec mixing time with a ^{15}N spinlock of 21 kHz (both NAL and NAVL). The PMPT experimental cross-peaks are from the 10 msec mixing time with the indicated ^{15}N spinlock for NAL and the optimized ^{1}H spinlock used in Figure 11. For NAVL, the PMPT experiment used the 10 msec mixing time with ^{1}H and ^{15}N spinlocks of 65.8 and 57.5 kHz, respectively (same as in Supplementary Figure 19). It is not appropriate to compare the intensities between NAL and NAVL, as the crystal sizes were different.

NIH-PA Author Manuscript NIH-PA Author Manuscript NIH-PA Author Manuscript

NIH-PA Author Manuscript

NIH-PA Author Manuscript

NIH-PA Author Manuscript

Table I

The average of intensity values per unit time for NAL and NAVL as plotted in Figure 14. The third column shows the data further normalized to 1.0 for the experiment that gave the most intensity / time in NAL and NAVL.

NAL	Intensity / Time	Normalized
PDSD (2 sec)	0.5	0.0069
PDSD (10 sec)	1.2	0.017
PDSD (30 sec)	2.1	0.029
CRDSD	50.1	0.70
PMPT (21 kHz)	72.0	1.0
PMPT (37.5 kHz)	55.1	0.77
PMPT (52.5 kHz)	40.6	0.56

NAVL	Intensity / Time	Normalized
PDSD (2 sec)	15.7	0.81
PDSD (4 sec)	19.5	1.0
PDSD (10 sec)	10.1	0.52
CRDSD	2.8	0.14
PMPT	5.5	0.28